Evolution of precipitates in lead-implanted aluminum: A backscattering and channeling study

K. K. Bourdelle*
Niels Bohr Institute for Astronomy, Physics and Geophysics, Ørsted Laboratory, Universitetsparken 5, DK-2100 Copenhagen Ø, Denmark

V. A. Khodyrev
Institute of Nuclear Physics, Moscow State University, 119899 Moscow, Russian Federation

A. Johansen, E. Johnson, and L. Sarholt-Kristensen
Niels Bohr Institute for Astronomy, Physics and Geophysics, Ørsted Laboratory, Universitetsparken 5, DK-2100 Copenhagen Ø, Denmark
(Received 13 January 1994)

The behavior of lead atoms implanted at 150 keV into (110) aluminum single crystals is studied by Rutherford backscattering (RBS) and a channeling technique. Channeling observed for the Pb signal in the as-implanted samples for implantation fluences in the region of 1×10^{15}–3.1×10^{16} cm^{-2} is ascribed to the formation of nanometer-sized Pb inclusions growing in topotaxy (epitaxy in three dimensions) within the Al matrix. Monte Carlo channeling simulations have been performed based on average sizes of the inclusions obtained from transmission electron microscopy and depth distributions of Pb atoms from RBS. It was shown that channeling in the inclusions strongly depends on their size. Large inclusions demonstrate by far the best channeling due to the relative reduction of the surface (interface) peak effect. In the simulations multiple intersections of the inclusion/matrix interfaces were found to be of importance for dechanneling of the analyzing ions. Comparison of the simulations with experimental data showed that in the as-implanted samples a considerable fraction of the Pb atoms is in supersaturated solution and in small ($\leq$ 1 nm) inclusions which do not show significant channeling. Upon annealing the larger inclusions grow by absorption of atoms from the solution and coalescence with smaller precipitates. It is shown that the inclusions grow nearly perfectly aligned with the Al matrix in a cube-cube orientation relationship and with a possible misorientation of less than 0.1°. Features related to the coherency of the inclusion/matrix interface are discussed and a comparison with other channeling measurements for nanometer-sized crystallites is made.

I. INTRODUCTION

Precipitation phenomena due to spontaneous phase separation in immiscible or nearly immiscible alloys have attracted the attention of scientists for a long time. They are of considerable interest in both applied and fundamental research. For example, the behavior of helium and other inert gas bubbles in fusion and fission reactor materials together with associated radiation damage significantly determines reactor lifetimes.[1] Creation of buried layers in metals by ion beams develops via formation of inclusions of a new phase and their successive agglomeration.[2] In microelectronics the precipitation of implanted B and Sb dopants in silicon is of importance in predictions of dopant redistributions during annealing.[3]

From a fundamental point of view the behavior of small assemblies of atoms gives a possibility to study many physical phenomena such as diffusivity and growth, melting and solidification of inclusions, etc. The lack of a free surface for nanometer-sized crystalline precipitates results in a range of physical properties which may differ considerably from those for the same bulk materials and for free nanometer-sized crystallites. An example is the exciting discovery of solid inclusions of the heavier inert gases implanted into different metals at room temperature (RT).[4,5]

Lead is practically insoluble in aluminum, having a solubility in the liquid phase as low as 0.19 at. %.[6] The early study of this system, made by Thackery and Nelson[7] using transmission electron microscopy (TEM) and electron diffraction, showed that implantation of Pb^+ ions at concentrations of about 5–15 at. % results in the formation of nanometer-sized Pb precipitates aligned in topotaxy with the aluminum matrix. They observed that the inclusions did not grow significantly at annealing temperatures below 290 °C. For samples implanted at elevated temperatures the inclusions were larger than those formed after implantation at RT.

X-ray diffraction (XRD) studies[8,9] of lead precipitates in implanted aluminum crystals showed that they grow topotactically in the matrix with a cube-cube orientation relationship. Unlike the highly pressurized noble gas inclusions the pressure in the Pb precipitates with a size about 14 nm was found to be less than 0.18 GPa. During melting, superheating of the Pb inclusions is significant, their melting point is size dependent, and the highest

0163-1829/94/50(1)/82(11)/$06.00

melting point was observed to be 67 °C above the bulk melting point of lead [328 °C (Ref. 6)]. The shape of the inclusions was determined to be a truncated octahedron with larger {111} and smaller {100} facets. Unfortunately, in these studies it was not possible to obtain information from the inclusions with sizes smaller than 5.5 nm.[8,9]

TEM data[11,12] obtained for polycrystalline samples with Pb^+ ions implanted at 100 keV in the fluence region 2×10^{15}–5×10^{16} cm^{-2} provided direct information about size distributions and areal densities of the precipitates. Precipitates with an average size (a distance a between opposite {100} facets of the inclusion was considered as a size) between 2.1 and 4.6 nm were observed after RT implantation. The average size increases gradually with fluence up to $\phi = 2\times10^{16}$ cm^{-2}. It was shown that the size distributions of the precipitates are rather narrow (standard deviation of about 1–2 nm for the lower fluences), but have a tendency to become wider at higher fluences. In Ref. 12 it was argued that the existence of the large inclusions (average size $\sim$ 14 nm for as-implanted samples) observed in the XRD experiments[8,9] may be attributed to accidental heating of the samples during the implantations.

In this work we combine an experimental channeling study of lead implanted into aluminum with Monte Carlo channeling simulations. This provides a possibility of investigation of some structural characteristics of the system Al matrix—Pb nanometer-sized inclusions at a quantitative level.

The paper is organized as follows. After this Introduction the experimental details are briefly described in Sec. II. A description of the Monte Carlo computer program used in the interpretation of channeling experiments together with some results of the simulations are presented in Sec. III. The experimental data for as-implanted samples and those obtained after isochronal thermal annealings are described in Sec. IV. The discussion of the experimental data together with the results of channeling simulations are situated in Sec. V.

Some of the experimental data presented in this work have been described in a Brief Report published previously.[10]

II. EXPERIMENTAL DETAILS

Single crystal aluminum disks 9 mm in diameter and 2 mm thick were spark cut perpendicular to a ⟨110⟩ or ⟨111⟩ direction from a larger crystal (Monocrystals Company, Cleveland, OH). The surfaces used for implantation were prepared by mechanical and electrolytical polishing showing minimum channeling yield (⟨110⟩ axial channel) of about 3% determined just below the surface peak for the virgin samples. The crystals were implanted at RT in an isotope separator with 150 keV Pb^+ ions to fluences in the range from 2.7×10^{14} to 3.1×10^{16} cm^{-2} using a beam current less than 2 μA cm^{-2}. In order to reduce effects of channeling during implantation the crystals were tilted 8° off normal incidence and rotated over the azimuthal angle.

Initial characterization of the samples was made *in situ* by Rutherford backscattering (RBS) and channeling techniques using a 500 keV He^{2+} beam from the separator. After implantation the crystals were annealed *in situ* at different temperatures between 250 and 480 °C without breaking the vacuum. The heating rate was dependent on annealing temperature T_a, and stable values of T_a were reached after 7–10 min heating from RT. After annealing, the samples were slowly cooled in such a way that the initial 100 °C decrease in temperature took place within the first 7 min. The annealing time was 1 h. Throughout these experiments a stable vacuum of 10^{-5} Pa was kept by turbomolecular pumping and a liquid nitrogen trap was used to suppress surface contamination of the samples.

Additional channeling measurements were made for several (110) Al samples at a HVEC 2-MeV Van de Graaff accelerator using 500 keV and 2 MeV He^+ beams. The angular position of the ⟨110⟩ axis was determined using a two-axis goniometer. Full circular azimuthal scans were performed for each new (increasing) polar tilt angle. This procedure allowed us to minimize the uncertainties due to effects of planar channeling. All channeling experiments were carried out at RT.

III. CHANNELING SIMULATIONS

Only the main features of the simulation procedure will be mentioned. The elaborate description of the Monte Carlo program UPIC used in this study will be published elsewhere.[13] For basics of Monte Carlo channeling simulations the reader is referred to the pioneering work of Barrett.[14]

In the simulations a crystal is divided into three-dimensional rectangular cells, each containing one atom.[13] We confine each step of the simulations to one of these cells in which the ion trajectories are calculated on the basis of a binary collision model in the impulse approximation using the Lindhard potential.[15] Electronic energy losses which are dependent on the impact parameter are taken into account. Thermal vibrations are simulated by Gaussian displacements of the Pb and Al lattice atoms around their equilibrium positions using the amplitudes from Ref. 16. In order to simulate azimuthal scans the initial velocities of the projectiles were uniformly distributed around the direction of the ⟨110⟩ axis with a fixed value of the polar tilt angle θ. The nuclear encounter probabilities averaged over all the followed trajectories are calculated as a function of depth for the Al and Pb atoms. The simulated data for tilt angles exceeding the corresponding values of the critical angles for channeling ψ_c (Ref. 15) are used for normalization when extracting the angular dependences of the normalized RBS yields $\chi(\theta)$.

A schematic illustration representing a projection of a single inclusion onto the $(1\bar{1}0)$ plane is shown in Fig. 1. We assume here that the ratio a/b, where b is the distance between opposite {111} facets of the inclusion, is 1.28 as deduced from the TEM measurements.[17] The volume of such a truncated octahedron is equal to the

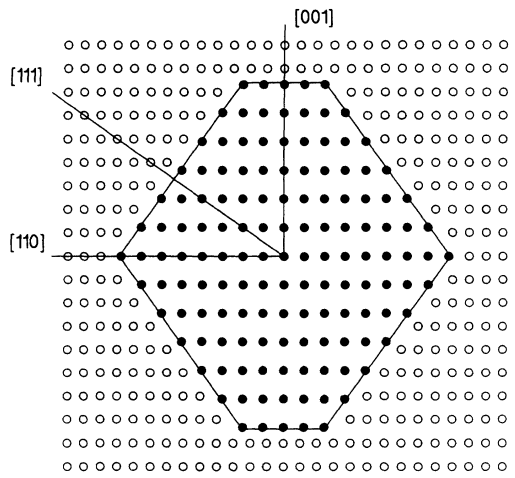

FIG. 1. Schematic illustration of a single Pb inclusion embedded in Al. The solid circles are Pb atoms and open circles are Al atoms.

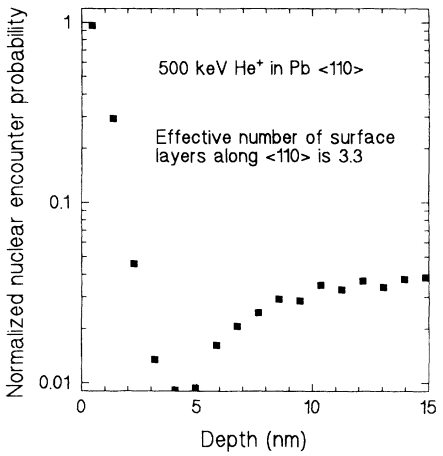

FIG. 2. Nuclear encounter probability calculated as a function of depth below the surface of lead crystal for axial channeling.

volume of a sphere with diameter d, when $d = 0.9072a$. In the simulations we consider the shape of the individual inclusion to be spherical with diameter d. We refer to the diameter of such sphere as the size of the inclusion.

The inclusions were assumed to be homogeneously distributed over the depth interval, where the main part of the implanted lead atoms was found by RBS. We assumed further that the inclusions for a given simulation are of equal size. The number of inclusions per unit volume was then calculated from the implantation fluence measured by RBS. The assumption of monodisperse size distributions looks reasonable, because channeling in the precipitates has a relatively smooth size dependence (see below), and contributions from opposite parts of the size distribution partially compensate each other. In any case, we do not have any data on the depth dependence of size distributions of the inclusions. The precipitates were assumed to be defect free.

Because of the large lattice mismatch of 22.2% between Al and Pb matrices (lattice constants are 4.05 Å and 4.951 Å for Al and Pb,[16] respectively) we consider in general that the matrix/precipitate interfaces are fully incoherent. In the simulations we assumed that the projectiles leaving an aluminum cell[13] at the matrix/precipitate interface enter the corresponding lead cell in a random transverse position. The same was supposed for the projectiles leaving the Pb inclusion at the opposite interface. In general it is assumed that the inclusions grow in topotaxy with aluminum matrix in a perfect cube-cube orientation relationship. It is supposed also that there are no strains either in the inclusion or in the matrix.

Due to the assumed incoherency of matrix/inclusion interfaces and the small (about some nanometers) size of the precipitates, the influence of the surface peak (for the inclusions embedded in a host matrix it should rather be named the interface peak) on channeling both in the Al matrix and the Pb inclusions must be of a crucial importance. The surface peak represents the contribution from the outermost (1–5) layers of a single crystal to the normalized nuclear encounter probability—the minimum channeling yield.[14] The contribution from, e.g., the first monolayer is typically two orders of magnitude higher than the contributions from the bulk layers. The results of the simulations of the depth dependence of the normalized nuclear encounter probability for 500 keV He^+ ions incident along a ⟨110⟩ axial direction of a Pb single crystal are shown in Fig. 2. The effective number of surface layers contributing to the surface peak is about 3.3.

To illustrate this point further the solid line in Fig. 3

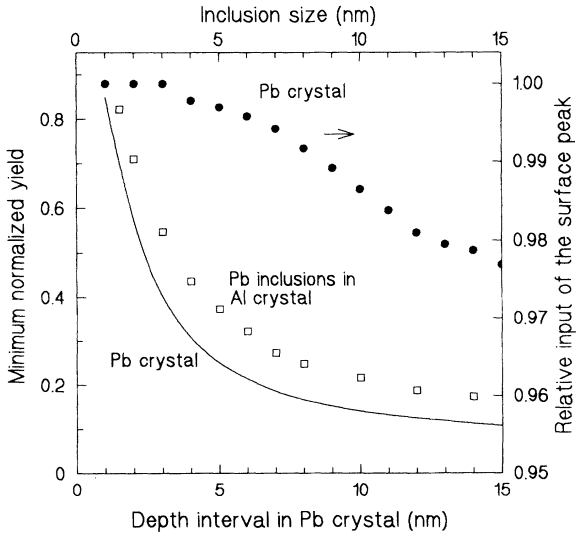

FIG. 3. The solid line shows the values of $\chi_{min}^{c\text{-}Pb}$ as a function of the depth interval Δz. The solid dots represent the Δz dependence of the relative contribution of the surface peak to $\chi_{min}^{c\text{-}Pb}$ (see text for details). The squares show the simulated values of the minimim yield for monodisperse distributions of Pb precipitates embedded in an Al matrix as a function of the inclusion size. The values of χ_{min}^{prec} were integrated over the depth interval 30–160 nm. All simulations are performed for 500 keV He^+ ions aligned along the ⟨110⟩ axis in Pb and Al crystals.

shows the simulated values of the minimum yield in a Pb single crystal χ_{min}^{c-Pb} as a function of the depth interval Δz (starting from $z = 0$) over which they are averaged (these data are extracted from Fig. 2). The solid dots in Fig. 3 represent the Δz dependence of the relative input of the surface peak (yield in the depth region 0–30 Å as shown in Fig. 2) to the χ_{min}^{c-Pb}. It is seen that the surface peak dominates the channeling yield in a Pb single crystal for the depth intervals up to 15 nm.

To illustrate the channeling effect in Pb inclusions of different sizes, the open squares in Fig. 3 show the simulated values of the minimum yield for assemblies of equal size Pb precipitates embedded in the Al matrix χ_{min}^{prec} as a function of their size. The values of χ_{min}^{prec} are obtained with the following parameters: The inclusions are distributed in the Al matrix over the depth region 30–160 nm, and the total amount of lead atoms confined within each assembly is 1.8×10^{16} cm^{-2}. It is seen that a size dependence of χ_{min}^{prec} resembles the Δz dependence of minimum yield for a Pb crystal and good channeling (χ_{min}^{prec} less than 70%) is observed only for inclusions with sizes greater than about 2 nm due to the interface peak effect. It is also seen that channeling in the lead precipitates is little influenced by the motion of the analyzing ions through the aluminum matrix. This is due to a significantly larger critical angle ψ_c ($\psi_c \propto \sqrt{Z_2}$, where Z_2 is atomic number of target atom) for channeling in the Pb crystal as compared with aluminum.[15]

Figure 4 demonstrates the effect of the presence of Pb inclusions on channeling in aluminum. The solid dots in Fig. 4 correspond to the ⟨110⟩ axial channeling dip for a virgin Al crystal obtained over the depth interval 30–160 nm. The results of simulations of ⟨110⟩ channeling dips in Al matrices containing assemblies of precipitates with monodisperse size distributions with $d = 1.5$ and 5 nm are shown in Fig. 4 with the open squares and stars, respectively. Here we again assume that the inclusions are homogeneously distributed over the depth interval 30–160 nm and the amount of Pb atoms confined within each assembly is 1.8×10^{16} cm^{-2}. For assemblies of inclusions containing an equal amount of Pb atoms the average number of interface intersections is inversely proportional to d, while the average path length of the projectiles within the inclusions is independent of d. Therefore, for an assembly with smaller inclusion size the role of the interface intersections is increased and the difference between channeling dips obtained for $d = 1.5$ and 5 nm is attributed to the influence of the precipitate/matrix interface on the dechanneling in the Al matrix. The dechanneling induced by the inclusions is of importance when discussing the evolution of implantation-induced damage in aluminum.

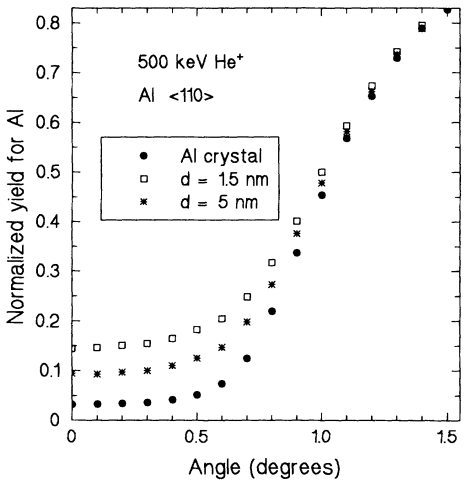

FIG. 4. The solid dots show simulated axial channeling dip for a virgin Al crystal. Two other channeling dips are calculated for Al crystals in which the assemblies of lead inclusions with size $d = 1.5$ nm (open squares) and 5 nm (stars) are embedded (see text for the other input parameters used in the simulations).

IV. RESULTS

A. Results for as-implanted samples

The as-implanted Pb depth profiles obtained from the experimental RBS spectra by applying standard formulas[18] for fluences up to 3.1×10^{16} cm^{-2} are shown in Fig. 5. Here the solid lines correspond to implantation into (110) Al and the dashed line to (111) Al crystals. A close inspection of these profiles shows that for fluences up to 1.8×10^{16} cm^{-2} the retained fraction of lead is about 100%. Figure 6 shows a comparison between the experimental and simulated [obtained from TRIM-91

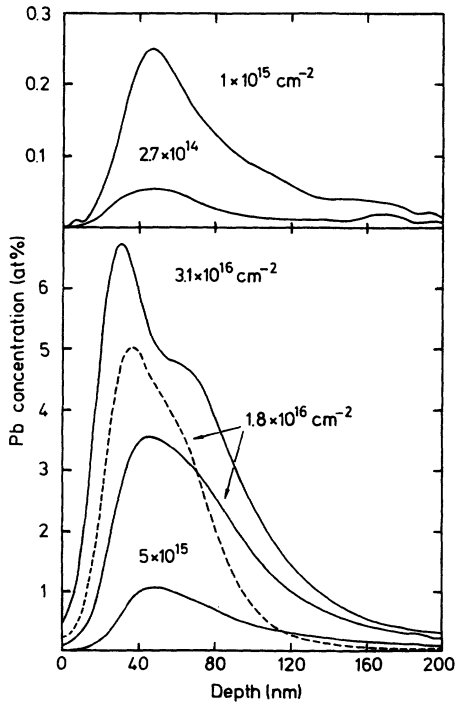

FIG. 5. Pb depth profiles measured after 150 keV implantation into aluminum at RT. Solid lines correspond to implantation into (110) crystals, dashed line to (111) crystal. All implantations have been performed 8° off normal incidence. The lines represent polynomial fits to the experimental data.

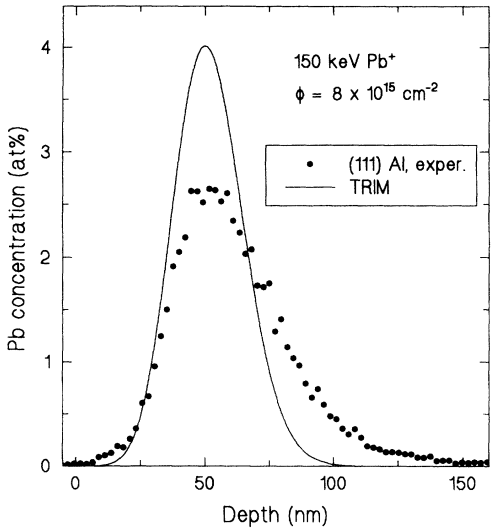

FIG. 6. Experimental Pb depth profile for (111) Al crystal (solid dots). Solid line is a theoretical profile obtained from TRIM-91 program and convoluted with the experimental depth resolution function.

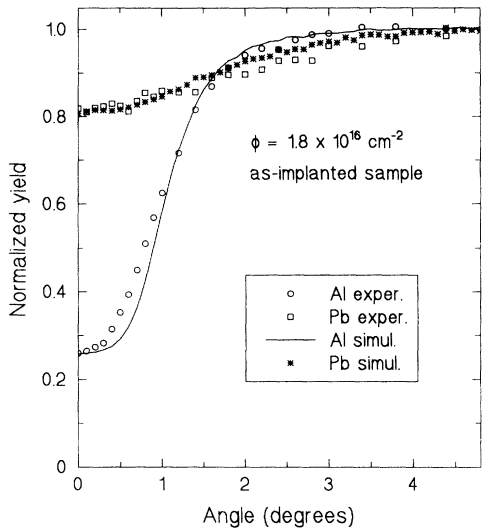

FIG. 8. Angular yield curves of 500 keV He^+ ions backscattered from an Al crystal implanted with lead. Both experimental and simulated channeling dips were obtained for the depth region 30–110 nm. The simulations were done assuming that 35% of implanted Pb atoms are in precipitates with a size of 3.8 nm, and the rest of Pb atoms are randomly displaced in the Al matrix. 19% of the Al atoms were supposed to be randomly displaced from the perfect lattice sites in the depth region 0–110 nm in order to fit experimental data for aluminum.

(Ref. 19)] depth profiles. The simulated profile was convoluted with the experimental depth resolution function.

The dependence of the minimum normalized yields for the Al and Pb signals—χ_{min}^{Al} and χ_{min}^{Pb}—as a function of fluence for ⟨110⟩ channeling of the 500 keV He^{2+} beam is shown in Fig. 7 for the as-implanted samples. These values were obtained for the depth region up to 200 nm. The χ_{min}^{Al} is seen to increase gradually with the fluence. Weak channeling was found in the lead already for a fluence of 1×10^{15} cm^{-2}. Furthermore we observe that χ_{min}^{Pb} decreases with increasing fluence.

Figure 8 shows lead and aluminum ⟨110⟩ axial channeling dips for the sample implanted with $\phi = 1.8\times10^{16}$ cm^{-2}. These dips were obtained for the depth region

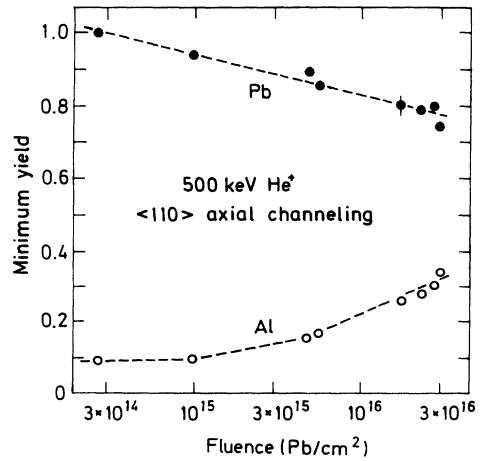

FIG. 7. Minimum yields from Pb and Al atoms measured for as-implanted samples as a function of the implantation fluence. The values of χ_{min}^{Al} and χ_{min}^{Pb} were obtained for the depth interval up to 200 nm. The dashed lines through the data points are drawn to guide the eye.

30–110 nm, which corresponds to the central part in the Pb distribution as shown in Fig. 5. It is seen that the channeling dip for Pb is substantially wider than for Al.

B. Isochronal annealing experiments

It was shown[10,12] for the samples implanted with $\phi = 1.8\times10^{16}$ cm^{-2} that the main changes in channeling both in the lead and aluminum signals occur after the first 15–30 min of annealing in the temperature interval 250–480 °C. Isothermal annealings for larger time intervals demonstrate that a rather steady state with little improvement of the channeling is reached. The kinetics of annealing for the samples implanted with lower fluences are similar to those for $\phi = 1.8\times10^{16}$ cm^{-2}. The data presented below are obtained after isochronal annealings for 1 h.

Figure 9 shows the measured values of the χ_{min}^{Pb} and χ_{min}^{Al} ($\phi = 1.8\times10^{16}$ cm^{-2}) as a function of annealing temperature. Annealing at 250 °C does not cause significant improvement in channeling either in the Al or Pb signals, and no redistribution of lead in the Pb depth profile was found. At 330 °C there is a pronounced decrease in χ_{min}^{Pb} which is accompanied by some Pb segregation (less than 1% of the total amount of implanted lead atoms) to the surface. It is seen in Fig. 9 that annealing at 380 °C leads to significant changes both in χ_{min}^{Pb} and χ_{min}^{Al} as compared with as-implanted samples. For the sample implanted with $\phi = 1.8\times10^{16}$ cm^{-2} there is still little redistribution of lead as observed by RBS (about

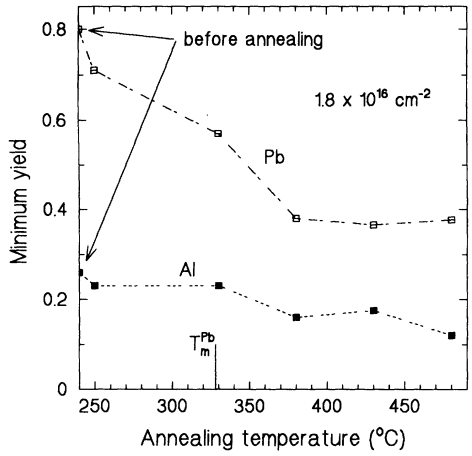

FIG. 9. The values of χ_{min}^{Al} and χ_{min}^{Pb} measured for the depth region up to 200 nm before and after annealings of the samples at different temperatures. The data represent the average values obtained after measurements for several (2–3) samples implanted and annealed at the same conditions. The dashed lines through the data points are drawn to guide the eye. The vertical line shows the bulk melting point of lead.

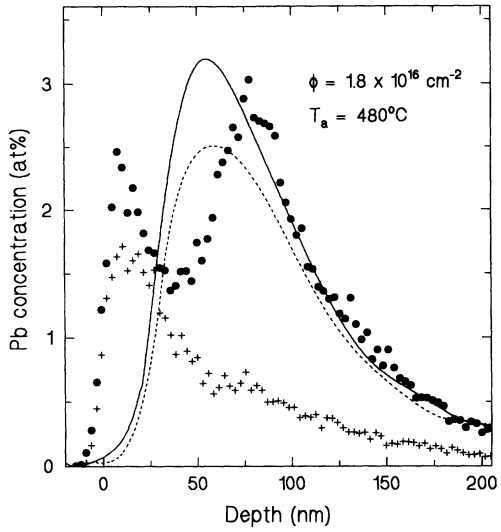

FIG. 11. Lead depth profiles before (lines) and after (solid dots and crosses) annealing at 480 °C measured at random (solid line and solid dots) and aligned (dashed line and crosses) incidence of 500 keV He^{2+} beam. The profiles for the as-implanted sample represent polynomial fits to the experimental profiles.

2% of implanted Pb atoms segregate to the surface); however, annealing at 380 °C of the sample implanted with $\phi = 1\times10^{15}$ cm^{-2} is characterized by strong segregation of Pb where a distinct peak in the vicinity of the surface (depth region 0–15 nm) is formed as shown in Fig. 10.

Annealings at 430 and 480 °C do not cause a further decrease of χ_{min}^{Pb} but result in some decrease of χ_{min}^{Al} as shown in Fig. 9 (at lower fluences the damage in the Al matrix as seen by channeling is completely annealed out). Figure 11 depicts the lead profiles measured by RBS analysis at random and channeling incidence of the analyzing beam before and after annealing of the sample implanted with $\phi = 1.8\times10^{16}$ cm^{-2} at 480 °C. The transport of Pb atoms to the surface is clearly seen to be accompanied by depletion of lead in the region of initial maximum concentration. At the same time there is some increase of the Pb concentration at larger depth.

Detailed analysis of the lead profiles measured both under random and channeling incidence of the analyz-

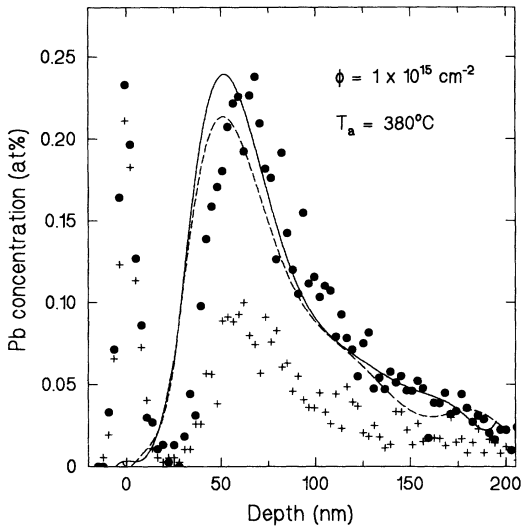

FIG. 10. Lead depth profiles before (lines) and after (solid dots and crosses) annealing at 380 °C measured at random (solid line and solid dots) and aligned (dashed line and crosses) incidence of 500 keV He^{2+} beam. The profiles for the as-implanted sample represent polynomial fits to the experimental profiles.

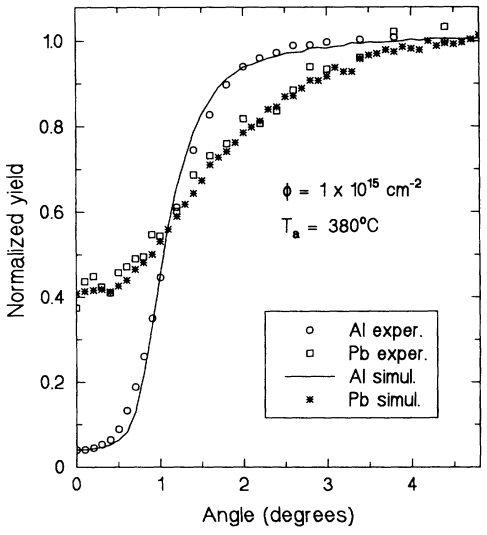

FIG. 12. Angular yield curves of 500 keV He^{+} ions backscattered from an Al crystal implanted with lead after annealing at 380 °C. Both experimental and simulated channeling dips are obtained for the depth interval 40–140 nm. The simulated Pb channeling dip was obtained with lead inclusions having a size of 4.3 nm (see text for other parameters used in simulations).

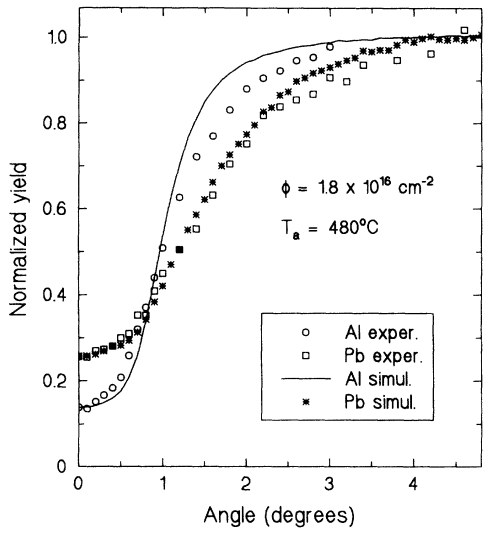

FIG. 13. Angular yield curves of 500 keV He^+ ions backscattered from an Al crystal implanted with lead after annealing at 480 °C. Both experimental and simulated channeling dips are obtained for the depth interval 40–160 nm. The simulated Pb channeling dip was obtained with lead inclusions having a size of 8 nm (see text for other parameters used in simulations).

ing beam shows that after annealing at temperatures between 380 and 480 °C two regions can be selected. In the surface region where lead is accumulated, the Pb atoms show little channeling, but in the deeper regions channeling increases significantly and χ_{min}^{Pb} approaches values of about 0.2–0.4.

Figure 12 shows aluminum and lead ⟨110⟩ axial channeling dips for a sample implanted with $\phi = 1\times10^{15}$ cm^{-2} and annealed at 380 °C, measured with a He^+ beam of 500 keV energy. These scans have been performed for the depth region of 40–140 nm, where the best channeling for lead has been observed. The ⟨110⟩ axial channeling dips obtained for a sample implanted with $\phi = 1.8\times10^{16}$ cm^{-2} and annealed at 480 °C are shown in Fig. 13. The scans have been performed for the depth region 40–160 nm.

V. DISCUSSION

A. As-implanted case

Comparison of the Pb profiles for (110) and (111) crystals implanted (8° off normal incidence and rotation over the azimuthal angle) with the same fluence in Fig. 5 clearly demonstrates the influence of channeling effects on the depth distribution of Pb atoms. For (110) crystals it is particulary difficult to avoid accidental planar channeling during implantation, because the ⟨110⟩ axis in the fcc structure is the most closely packed. The second peak in the Pb distribution observed in Fig. 5 for the lowest fluence implantation is believed also to be due to channeling. Nevertheless, the broadening of the experimental depth profile found for the (111) crystal as compared with the simulated profile (Fig. 6) seems to be too large to be explained by channeling effect alone. We conclude that during implantation some migration of Pb atoms has also occurred. The shift in peak position of Pb towards the surface at the highest fluence is due to sputtering.[20]

It was observed[21] that Pb atoms implanted into Al at 5 and 27 K might occupy substitutional sites, while RT implantation in contrast leads to zero substitutionality. One can hardly expect Pb atoms to occupy an interstitial site in an fcc metal. Most probably Pb-vacancy complexes PbV_m, where m = 2–5, are formed, resulting in significant displacement of the Pb atoms from the perfect lattice sites.[21] The complexes distort the Al lattice and some part of the damage observed in the Al matrix with the channeling technique may be due to this effect. A decrease of χ_{min}^{Pb} with fluence in Fig. 7 is therefore intriguing, especially as it is accompanied by a steady increase in χ_{min}^{Al}. The puzzle is resolved by observation of a considerably wider channeling dip for the Pb signal in Fig. 8 that is clearly associated with a channeling effect in the lead precipitates. Formation of precipitates at fluences exceeding the value of 3×10^{14} cm^{-2} gives further evidence that Pb atoms are highly mobile during evolution of the collision cascade. Their motion is assisted by radiation-induced vacancies, and inclusions are presumed to nucleate on multivacancy complexes.

It can be concluded from Fig. 3 that the Pb atoms within inclusions with a size less than about 1 nm (this is also the practical detection limit of TEM measurements[12]) do not give any contribution to channeling in the Pb signal. The Pb atoms may also form clusters, i.e., agglomerates of several Pb atoms where the aligned beam of the analyzing ions will see the atoms within the Pb clusters to be randomly displaced. We refer to individual Pb atoms in supersaturated solution (see discussion above), the Pb atoms in clusters and small (d < 1 nm) precipitates as the random fraction of Pb atoms ν. The rough estimates of ν were obtained from TEM data for the as-implanted samples where ν varied from 36% up to 66% of the retained dose depending on the fluence.[12]

The results of the channeling simulations for the sample implanted with $\phi = 1.8\times10^{16}$ cm^{-2} are shown in Fig. 8. To fit our simulations to the experimental Pb channeling dip we have used two parameters: the size of the inclusions d (see Sec. III) and the random fraction ν. The dechanneling due to the random fraction was calculated by setting the appropriate number of single Pb atoms to be randomly distributed over the volumes of the empty aluminum cells (see Sec. III), and these Pb atoms were supposed to give $\chi^{Pb}(\theta) = 1$ to the normalized yield for the Pb signal. The simulated Pb channeling dip depicted in Fig. 8 was obtained assuming d = 3.8 nm and ν = 0.65. These values are in good agreement with those from TEM: about 4 nm (average size) and about 65%, correspondingly.[12] However, due to two parameters used in the simulations the same fit (in statistical limits of our simulations) to the experimental data can be obtained with $d = 3.8\pm0.6$ nm and ν within interval 0.60–0.68.

The simulated Al channeling dip shown in Fig. 8 was obtained assuming that 19% of the Al atoms are ran-

domly displaced from the perfect lattice sites in the depth region 0–110 nm. As we have earlier pointed out[10] this is not a true measure for a point defect concentration but a value of a free parameter which fits the observed damage-induced dechanneling in the Al matrix. The simulations have shown that this value has little influence on channeling in the inclusions.

The results on the fluence dependence of channeling in lead shown in Fig. 7 may be explained as due to an increase in the average size of the inclusions with increase of ϕ, and the sizes in the range 1.7–4.0 nm (random fraction 60–70%) can be deduced from simulations for the fluence region 1×10^{15}–3.1×10^{16} cm^{-2}. We conclude that the as-implanted samples represent a metastable system with the inclusions and a random fraction of Pb atoms embedded in a heavily damaged Al matrix.

B. Structural changes after annealing

Results depicted in Fig. 9 for the sample implanted with $\phi = 1.8\times10^{16}$ cm^{-2} and annealed at 250 °C show that neither aluminum lattice defects nor Pb atoms in random fraction and Pb inclusions are significantly mobile at this temperature. Annealing at 330 °C, when nearly all of the inclusions are solid,[9] results in significant improvement of the channeling in the Pb signal, but almost no depth redistribution of Pb as measured by RBS is observed. This temperature corresponds to an activation energy of 1.55 eV, which is close to the value found for tracer diffusion of Pb in Al: $Q = 1.51$ eV.[22] The extrapolation of data[22] gives D of about 1.2×10^{-11} cm^2 s^{-1} for 330 °C with the characteristic diffusion length $\sqrt{Dt}$ of about 800 nm for $t = 10$ min. The small redistribution of the implanted Pb atoms we observed at this temperature may be qualitatively explained as follows.

A considerable amount of Pb atoms in the as-implanted samples are confined within the inclusions. The migration of these inclusions may be described either in terms of a volume diffusion mechanism, where transport of vacancies through the matrix controls the precipitate motion or by surface diffusion mechanism, where the host atoms are migrating at the inclusion/matrix interface. From the study of gas bubble migration in metals the following relationship can be deduced:

$$D = \frac{6\Omega}{\pi d^3} D_v \tag{1}$$

for volume diffusion control[1] and

$$D = \frac{24\Omega^{4/3}}{\pi d^4} D_s \tag{2}$$

for surface diffusion control.[23] Here, Ω is the atomic volume of the matrix, D_v is the vacancy diffusion coefficient (see data for aluminum in Ref. 24), and D_s is the interface self-diffusion coefficient of the matrix atoms. The use of Eq. (1) assuming precipitates with $d = 5$ nm gives diffusion coefficients for the Pb inclusions which are about five orders of magnitude lower than those for tracer diffusion from Ref. 22. The experimental data of Van Siclen *et al.*[25] for diffusion of helium bubbles covered with a thin layer of melted Pb, which have been interpreted in terms of surface diffusion mechanism, provide $D = 2\times10^{-14}$ cm^2 s^{-1} for a bubble with d about 10 nm in the temperature interval 450–470 °C. The strong interaction expected between surface (at the inclusion/matrix interface) defects and solid Pb precipitates might result only in a decrease of D as compared with values from Eq. (1) and corresponding extrapolation of data in Ref. 25. Therefore, regardless of whether the inclusions move by volume or surface diffusion control we conclude that the lead precipitates are immobile at 330 °C. They represent a dense network of traps (the average distance between the inclusions is much smaller than the thickness of the implanted layer[12]) which can capture the mobile Pb-vacancy complexes and Pb clusters. The decrease of $\chi_{\min}^{Pb}$ after annealing at this temperature is explained to be due to a reduction of the random fraction of lead atoms.

Increase of T_a results in a stronger redistribution of Pb and a considerable increase of channeling in the lead signal as shown in Figs. 10 and 11. The results of channeling simulations shown in Fig. 12 (solid line and stars) for the sample implanted with $\phi = 1\times10^{15}$ cm^{-2} and annealed at 380 °C were obtained with the following parameters: Randomly displaced Pb atoms with a concentration of 0.15 at.% are distributed within the interval $z = 0$–20 nm, while in the interval $z = 40$–140 nm the lead atoms are confined solely to the Pb inclusions with $d = 4.3$ nm. We assume that 0.5% of the Al atoms are randomly displaced in the depth region 0–140 nm. It is seen in Fig. 12 that the simulated channeling dips are in a good agreement with the experimental data.

The simulated channeling dips for a sample implanted with $\phi = 1.8\times10^{16}$ cm^{-2} and annealed at 480 °C are shown in Fig. 13. Here the fit to the experimental data was obtained using the following parameters: Pb atoms with a concentration of 2 at.% are randomly displaced in the depth region 0–30 nm (see Fig. 11), and at greater depth Pb atoms are confined solely to the Pb crystallites with a size of 8 nm, which are distributed over a depth interval of 30–160 nm. We obtain a $\chi_{\min}^{Al}$ value of about 7.5%, when considering a damage free Al matrix with dechanneling due to inclusions only (see Fig. 4). Therefore, in order to fit the experimental values of $\chi_{\min}^{Al}$, we assumed that 5.4% of the Al atoms are randomly displaced in the depth interval 0–160 nm. The correspondence between the simulated and the experimental channeling dips is not so good at larger tilt angles. That might be associated with experimental uncertainties.

In the simulations for the annealed samples we used low concentrations of displaced Pb and Al atoms which have little influence on simulated values of $\chi_{\min}^{Pb}$ that are almost entirely determined by the assumed size within the given assembly of inclusions. It is seen that the values of d obtained from channeling simulations for the annealed samples are about a factor 2 larger than those for the as-implanted samples. The absorption of the random fraction, i.e., about 60–70% of implanted Pb atoms, by larger inclusions might explain up to 40% of this increase (monodisperse size distributions of the precipitates before and after annealing are assumed). The results of the

simulations for the sample implanted with $\phi = 1.8\times10^{16}$ cm^{-2} (T_a = 480 °C) seem to be in some disagreement with TEM data,[12] where the average size of inclusions of 4.8 nm was obtained for the sample implanted with $\phi = 2\times10^{16}$ cm^{-2} and annealed at 380 °C for 1 h. These discrepancies might be explained as follows.

We believe that after annealings at $T_a \geq 330$ °C the random fraction of Pb atoms is absorbed by larger inclusions and segregate to the surface during the first minutes of annealing. The surface acts as a trap for Pb atoms. We will not discuss the mechanisms of the surface segregation in this paper. A relative influence of these two processes on the observed Pb redistribution is strongly dependendent on the fluence and hence on the average size of the inclusions. The effect of segregation is more pronounced after isothermal annealings of the samples implanted with lower fluences, where the average size of the inclusions is smaller. This effectively reduces the probability for the moving Pb cluster or single atoms to be trapped by the precipitates, because the areal density of the inclusions for as-implanted samples has little dependence on fluence.[12] The segregation explains the poor channeling in the Pb signal in the surface region. Therefore, after annealing, the deeper region where the main part of implanted Pb atoms is situated becomes essentialy free from the random fraction. This provides a significant improvement of channeling in Pb signal for that depth region. At $T_a \geq 380$ °C motion of small (d about 1–2 nm) inclusions might be activated [smaller inclusions are essentially more mobile than the larger ones as follows from Eqs. (1) and (2)] as can be seen from the channeling measurements presented, e.g., in Fig. 11. The drift of smaller precipitates towards the surface effectively gives a relative enrichment of the deeper region with larger inclusions. This might explain the disagreement between channeling and TEM data, because the last method gives size distributions of the inclusions averaged over depth (starting from the surface).

A significant part of an increase in the average size of the inclusions after annealings at $T_a \geq 380$ °C found by channeling analysis is believed to be due to absorption of mobile small precipitates by larger ones. A relatively low mobility of larger inclusions formed in deeper regions may explain the rather constant values of χ_{min}^{Pb} found after annealings in the temperature interval 380–480 °C (Fig. 9) and the little improvement of channeling in the lead signal observed after isothermal annealings for $t >$ 1 h.[10,12]

C. Mosaic spread, correlated interface, and comparison with other channeling measurements

An interesting problem is a possible mosaic spread of the inclusions. It is difficult to extract information about the value of the mosaic spread from the experimental data either by x-ray diffraction where the width of a corresponding diffraction peak is greatly affected by parameters related to the size distribution[9] or TEM technique. The last method gives an upper limit for the mosaic spread (relative misorientations of moiré fringes observed in TEM pictures were measured) of about 0.5° for the inclusions with size of 7–8 nm.[17] Figure 14(a) shows the simulated Pb angular dip for 500 keV He^+ depicted in Fig. 13 (no mosaic spread) together with the dips simulated with the same input parameters but now assuming that the inclusions have a mosaic spread (standard deviation) of 0.5°, 1.0°, and 2.0°, respectively. It is seen that introduction of mosaic spread leads to poorer channeling in the inclusions (20% increase in χ_{min}^{Pb} for mosaic spread of 0.5°) and to a certain increase in the half-widths of the corresponding channeling dips.

An increase in the sensitivity of the channeling measurements to the possible mosaic spread of the inclusions is achieved by increasing the energy E of the analyzing beam and therefore decreasing the critical angle ψ_c.[15] The experimental Pb channeling dip for the sample implanted with $\phi = 1.8\times10^{16}$ cm^{-2} (T_a = 480 °C) obtained with 2 MeV He^+ ions is shown in Fig. 14(b). The corresponding simulated dips (see Sec. IV B for the input

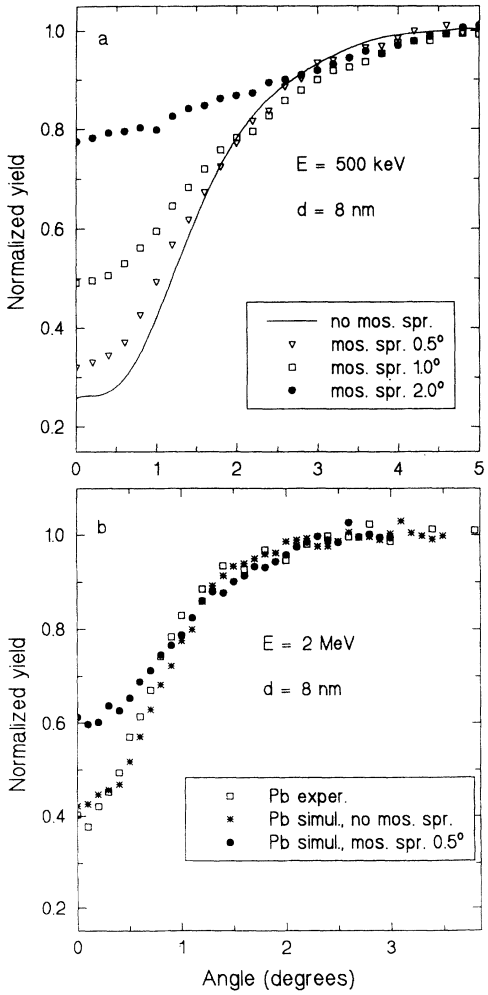

FIG. 14. (a) Simulated lead channeling dips (E = 500 keV) for inclusions having different mosaic spread (see text). The dip for zero mosaic spread is a polynomial fit to the simulated Pb channeling dip shown in Fig. 13. (b) Experimental lead channeling dip (see text) together with the simulated dips obtained with 2 MeV He^+ beam. All dips are obtained for the depth interval 40–160 nm.

parameters) for $E = 2$ MeV (no mosaic spread and with mosaic spread of 0.5°) are also shown in Fig. 14(b). It is seen that channeling in the inclusions is strongly dependent on E and that an increase in E leads to higher values of $\chi_{\min}^{Pb}$ as is expected due to the increase in intensity of the surface (interface) peak with energy.[14] On the other hand, simulated values of $\chi_{\min}^{Al}$ [not shown in Fig. 14(b)] were found to be almost independent of energy, a result that is in a good agreement with our experimental observations. The introduction of a mosaic spread of 0.5° for $E = 2$ MeV leads to value of $\chi_{\min}^{Pb}$ which is 43% larger than that obtained with zero mosaic spread. A comparison of simulated Pb channeling dips with the experimental dip in Fig. 14(b) let us conclude that a value of the mosaic spread of Pb inclusions with an average size of about 8 nm is less than 0.1°. A subtle difference between experimental and simulated (zero mosaic spread) dips is attributed to the equal-size assumption used in our simulations.

So far we have considered the inclusion/matrix interface to be fully incoherent with no match between adjoining planes in the two phases. However, it might be assumed that due to the 22.2% lattice mismatch between Al and Pb approximately every fourth plane in the Pb lattice can match every fifth plane in Al, and therefore, the exit and inlet coordinates at the matrix/inclusion interface (see Sec. III) may be correlated. We have simulated this case but did not observe any difference (within statistical limits of our simulations) as compared to the noncorrelated interface.

To our knowledge there are only a few papers where channeling in nanometer-sized crystallites has been demonstrated.[10,26–29] Our preliminary results[10] obtained for the Pb precipitates in Al have been interpreted using channeling simulations based on the continuum model and assuming a statistical equilibrium. This model gave some estimates, e.g., of the random fraction of lead atoms and the mosaic spread in the inclusions. However, these estimates have a more qualitative character because the statistical equilibrium model does not take into account the features related to the finite size of the precipitates and the effects of the surface (interface) peak.

The other systems investigated were Pt precipitates in MgO,[26] and solid Kr inclusions in Al,[27–29] where poor channeling ($\chi_{\min}^{Kr}$ of about 0.9) was observed. No conclusions about the size or misorientation of the inclusions were drawn. The authors of Refs. 26–29 used an energy of the analyzing He^+ beams exceeding 1 MeV which might be not optimal for this kind of studies. Our previous discussion on the size and energy dependence of channeling in the inclusions is therefore of importance for the interpretation of, e.g., the results of Yagi *et al.*,[28,29] where according to TEM data[30] the solid Kr inclusions have an average size as small as 3 nm.

VI. CONCLUSIONS

For the first time an experimental channeling study of crystalline nanometer-sized inclusions is supplemented by extensive Monte Carlo simulations. The following conclusions based on this channeling analysis are reached.

Small lead crystallites are formed in the Al matrix during RT implantation of 150 keV Pb^+ ions for fluences larger than 3×10^{14} cm^{-2}. The inclusions have an average size of about 1.7–4.0 nm depending on the fluence, and about 60–70 % of the implanted Pb atoms are in supersaturated solution in association with vacancy complexes, in clusters, and in small ($d \leq 1$ nm) crystallites. That fraction of the Pb atoms does not demonstrate significant channeling.

During the first minutes of annealing at temperatures somewhat larger than 330 °C the random fraction of Pb atoms is absorbed either by existing inclusions or segregates to the surface. Therefore, after annealing at temperatures between 380 and 480 °C the Pb atoms in the deeper region ($z \geq 40$ nm) are confined solely to the inclusions. This results in a drastic improvement of channeling both for the Pb and Al signals, and an average size of the precipitates of about 7–9 nm is deduced from the simulations for the deeper region in the case of higher fluences. The inclusions are nearly perfectly aligned with the Al matrix in a cube-cube orientation relationship and a possible mosaic spread is less than 0.1°. No evidence for strain at the matrix/inclusion interface was found.

The results of the simulations show that channeling in the assemblies of lead inclusions embedded in the Al matrix is defined mainly by the properties of individual Pb precipitates, i.e., their size and misorientation with the matrix. The channeling analysis together with the TEM results where no distortion in moiré fringes have been found for Pb inclusions[12] let us conclude that the precipitates are essentially defect free. On the other hand the channeling in the Al matrix is largely determined by the spatial density and the size of the inclusions, and for the annealed samples implanted with higher fluences a substantial part of dechanneling in the Al matrix may be attributed to dechanneling at the inclusion/matrix interfaces.

The channeling analysis is shown to be a powerful technique for the study of nanometer-sized crystallites growing in topotaxy in crystalline matrices. Used in combination with other techniques it is possible to get important information about misorientation of crystallites, precipitate/matrix interface structure, possible lattice defects within the precipitates, melting and solidification of the inclusions, and their transport through the host matrix.

ACKNOWLEDGMENTS

We are grateful to B. Bech Nielsen, University of Aarhus, for provision of beam time and assistance with channeling measurements. L. Yu is acknowledged for taking part in early stages of experiments. We thank S. Steenstrup for the persistent help during implementation of the program UPIC on an IBM RISC System/6000 computer. This work was supported in part by the Danish Natural Science Research Council.

* On leave from Institute of Nuclear Physics, Moscow State University, 119899 Moscow, Russian Federation.
[1] P. Goodhew and S. K. Tyler, Proc. R. Soc. London A **377**, 151 (1981).
[2] D. W. Brown, R. G. Musket, and Z. A. Munir, Appl. Phys. Lett. **57**, 2651 (1990).
[3] S. Solmi, F. Baruffaldi, and M. Derdour, J. Appl. Phys. **71**, 697 (1992).
[4] C. Templier, C. Jaouen, J. P. Riviére, J. Delafond, and J. Grilhé, C. R. Acad. Sci. Paris II **299**, 613 (1984).
[5] A. vom Felde, J. Fink, Th. Müller-Hinzerling, J. Pflüger, B. Scherer, G. Linker, and D. Kaletta, Phys. Rev. Lett. **53**, 922 (1984).
[6] *Binary Alloy Phase Diagrams*, edited by T. B. Massalski, J. L. Murray, L. H. Bennett, and H. Baker (American Society for Metals, Metals Park, OH, 1986), Vol. 1, p. 147.
[7] P. A. Thackery and R. S. Nelson, Philos. Mag. **19**, 169 (1969).
[8] L. Gråbæk, J. Bohr, E. Johnson, H. H. Andersen, A. Johansen, and L. Sarholt-Kristensen, Phys. Rev. Lett. **64**, 934 (1990).
[9] L. Gråbæk, J. Bohr, H. H. Andersen, A. Johansen, E. Johnson, L. Sarholt-Kristensen, and I. K. Robinson, Phys. Rev. B **45**, 2628 (1992).
[10] K. K. Bourdelle, H. H. Andersen, A. Johansen, E. Johnson, L. Sarholt-Kristensen, S. Steenstrup, L. Yu, and B. Bech Nielsen, Nucl. Instrum. Methods B **64**, 143 (1992).
[11] B. Schmidt, K. Hjemsted, E. Johnson, K. K. Bourdelle, A. Johansen, H. H. Andersen, and L. Sarholt-Kristensen, Micron Microsc. Acta **23**, 215 (1992).
[12] K. K. Bourdelle, A. Johansen, B. Schmidt, H. H. Andersen, E. Johnson, L. Sarholt-Kristensen, S. Steenstrup, and L. Yu, Nucl. Instrum. Methods B **80/81**, 317 (1993).
[13] V. A. Khodyrev, V. Ya. Chumanov, K. K. Bourdelle, and G. P. Pokhil (unpublished).
[14] J. H. Barrett, Phys. Rev. B **3**, 1527 (1971).
[15] J. Lindhard, K. Dan. Vidensk. Selsk. Mat.-Fys. Medd. **34** (14) (1965).
[16] D. S. Gemmel, Rev. Mod. Phys. **46**, 129 (1974).
[17] B. Schmidt, M.Sc. thesis, Physics Laboratory, H. C. Ørsted Institute, University of Copenhagen, 1992.
[18] W. K. Chu, J. W. Mayer, and M. A. Nicolet, *Backscattering Spectrometry* (Academic, New York, 1978).
[19] J. F. Ziegler, J. P. Biersack, and U. Littmark, *The Stopping and Ranges of Ions in Solids* (Pergamon, New York, 1985).
[20] A. Johansen, E. Johnson, L. Sarholt-Kristensen, S. Steenstrup, L. Yu, and K. K. Bourdelle, Surf. Coat. Technol. **51**, 461 (1992).
[21] O. Meyer and A. Turos, Mater. Sci. Rep. **2**, 371 (1987).
[22] F. Sawayanagi and R. R. Hasiguti, J. Jpn. Inst. Met. **42**, 1155 (1978).
[23] D. R. Olander, *Fundamental Aspects of Nuclear Reactor Fuel Elements*, Publication No. TID-26711-P1 (National Technical Information Service, U.S. Department of Commerce, Springfield, VA, 1976).
[24] S. Dais, R. Messer, and A. Seeger, Mater. Sci. Forum **15-18**, 419 (1987).
[25] C. DeW. Van Siclen, R. N. Wright, and S. G. Usmar, Phys. Rev. Lett. **68**, 3892 (1992).
[26] A. Turos, O. Meyer, and Hj. Matzke, Appl. Phys. Lett. **38**, 910 (1981).
[27] H. H. Andersen, J. Bohr, A. Johansen, E. Johnson, L. Sarholt-Kristensen, and V. Surganov, Phys. Rev. Lett. **59**, 1589 (1987).
[28] E. Yagi, I. Hashimoto, and H. Yamaguchi, J. Nucl. Mater. **169**, 158 (1989).
[29] E. Yagi, Phys. Rev. Lett. **67**, 3804 (1991).
[30] R. C. Birtcher and W. Jäger, Ultramicroscopy **22**, 267 (1987).